J Therm Anal Calorim (2012) 108:1025–1031
DOI 10.1007/s10973-011-2043-2

The effect of carbonisation temperatures on nanoporous characteristics of activated carbon fibre (ACF) derived from oil palm empty fruit bunch (EFB) fibre

Wan-Cheng Tan · Radzali Othman · Akihiko Matsumoto · Fei-Yee Yeoh

ICVMTT2011 Conference Special Chapter

Abstract Activated carbon fibre (ACF) is a nanoporous material which is useful for various important applications such as safe biogas and natural gas storage as well as heavy/precious metals removal and recovery. It is commonly produced from synthetic fibres such as rayon, polyacrylnitrile and pitch mainly derived from petroleum products, which are less environmental friendly. Besides, cost of ACF production is high due to the high burnt off percentage of such expensive raw materials. As an alternative, natural fibre of oil palm empty fruit bunch was used as a raw material for ACF preparation. Thermogravimetric analysis was carried out with two different gases, i.e. nitrogen gas and oxygen gas in order to observe pyrolysis and combustion behaviours in different gases. Carbonisation temperatures were then identified from the peaks of derivative thermogravimetry results. Different carbonisation temperatures (85–200 °C) were chosen to carbonise the EFB fibre to observe the effect of carbonisation temperatures on the nanoporous characteristics, i.e. surface area, pore size distribution and pore volume of the ACF produced. Good nanoporous characteristics such as surface area up to 2,740 m^2/g of the ACF prepared were observed, suggesting EFB fibre as an excellent candidate to replace synthetic fibre for ACF production. The discussion of relationship between thermal characteristics and nanopores in ACF derived from EFB were also included in this study.

Keywords Activated carbon fibre Oil palm empty fruit bunch fibre · Thermogravimetric analysis Carbonisation temperature Pore characteristics

W.-C. Tan · R. Othman · F.-Y. Yeoh (✉)
School of Materials and Mineral Resources Engineering, Universiti Sains Malaysia, Transkrian Engineering Campus, Seri Ampangan, Nibong Tebal, Seberang Perai Selatan, 14300 Penang, Malaysia
e-mail: srfeiyee@eng.usm.my

A. Matsumoto
Department of Environmental and Life Sciences, Toyohashi University of Technology, Tempaku-cho, Toyohashi 441-8580, Japan

Introduction

Activated carbon attracted the interests from researchers [1–3]. Activated carbon fibre is a light porous carbon in a fibre shape. It is a nanoporous material with mainly micropores in its structure. The large pore volumes of the ACFs are contributed by their interconnected pores [4]. It offers short diffusion length with minimum pore diffusion resistance for adsorbates. It is widely used as a metal adsorbent and catalyst, safe biogas and natural gas storage, gas and liquid filtration, antibacterial wound dressings, disposable gas masks, water filtration and treatment, etc. Commonly, ACF produced from rayon [5, 6], polyacrylnitrile [7, 8] or pitch [9, 10]. Such petrochemical products are expensive and less environmental friendly. Besides the environmental concern, due to high burnt off percentages (more than 80%) of expensive raw materials [11] from petrochemical products, the cost of ACF remains a large barrier to be overcome in order to commercialise ACF for various applications.

Malaysia is one of the largest palm oil producer and exporter in the world [12]. More than 2.65 million hectares of land in Malaysia were used for oil palm cultivation [13]. The extraction of palm oil in oil mills left behind numerous lignocellulosic biomass as agricultural wastes, e.g. empty fruit bunch (EFB) fibre, palm kernel shell, mesocarp fibre and palm stone. Malaysia produces EFB fibre in substantial

amount, i.e. 20 million tonnes per year [14]. This fibre has very low market value. In fact, EFB fibre has natural pore channels where allows the access of fluid to nanopore generated on its pore wall. Thus, EFB fibre could be a good raw material in ACF production considering its cost, properties and environmental friendliness.

In this article, EFB fibre was selected as a raw material for ACF synthesis. Sulphuric acid and carbon dioxide gas were used as activating agents. The combustion and pyrolysis behaviours of EFB fibre were investigated by thermogravimetric analysis. The carbonisation temperatures were determined from thermogravimetry (TG) results. The effect of carbonisation temperatures on nanoporous characteristics of ACF was then studied.

Experimental

Empty fruit bunch fibre was obtained from a local palm oil mill in Penang, Malaysia, while sulphuric acid (H_2SO_4) was purchased from Merck for ACF synthesis. Dried, cleaned EFB fibre was treated with concentrated H_2SO_4. For carbonisation, the H_2SO_4-treated EFB fibre was then combusted at different temperatures identified from TG results. The carbonisation process was carried out in ambient at 85, 120, 130, 160 and 200 °C for 2 h without any external gas supply. After the heat treatments, the fibre was washed with deionised water to adjust its pH value and dried at 110 °C overnight. The fibre was further activated with CO_2 gas. This physical activation process was carried out by heating the fibre to 900 °C under N_2 atmosphere at a heating rate of 10 °C/min, followed by maintaining this temperature for 1 h under CO_2 gas stream (with the gas flow rate less than 1 L/min) and then cooled down to room temperature under N_2 atmosphere. Finally, ACF samples were obtained. The samples' code was tabulated in Table 1.

Thermogravimetric analyser (Q500 thermogravimetric analyser from TA Instruments Inc.) was used to analyse the thermal behaviours of EFB fibre and determine the carbonisation temperatures with heating rate of 5 °C/min in oxygen or nitrogen atmosphere in this study. The surface morphology and microstructure of the EFB fibre and ACF were analysed by using Zeiss Supra 35VP scanning electron microscope and energy dispersive spectrometer combination instrument. Nitrogen adsorption apparatus, namely Quantachrome autosorb instrument, was employed to measure physisorption of samples towards nitrogen at − 196 °C (77 K). The outgas temperature and duration were set at 300 °C and 3 h, respectively. For comparison with other works, the pore characteristics, i.e. specific surface area, micropore volume and pore size distribution of samples were calculated from the nitrogen adsorption isotherms by applying the Brunauer–Emmett–Teller (BET), Dubinin–Radushkevich (DR) and Horvath-Kawazoe (HK) models, respectively.

Table 1 Code of samples combusted in oxidative atmosphere

Sample's code	Carbonisation temperature/°C
EC85H2	85
EC120H2	120
EC130H2	130
EC160H2	160
EC200H2	200

Results and discussion

Thermogravimetric analysis

The thermal decomposition profile of raw EFB fibre in nitrogen supply was presented in Fig. 1a. Mass loss due to raw EFB fibre pyrolysis in nitrogen gas was categorised into three stages: moisture drying, main devolatilisation and continuous slight devolatilisation [15]. The moisture evaporated at temperature lower than 150 °C. No significant mass loss was observed in this region (0.06%) probably due to a low amount of surface adsorbed water by hydrophobic surface of EFB fibre. Even though most of the oil content in EFB fibre was rather low after extraction, there was still some residual oil content remaining in the EFB fibre. The surface of EFB fibre was rather hydrophobic with the oil content that prevented water adsorption from the atmosphere, hence only little mass loss was observed. The main devolatilisation regime initiated at ca. 200 °C and persisted to 350 °C with a mass loss of 49.54%. Beyond 200 °C, the mass decreased rapidly mainly because of devolatilisation of celluloses and hemicelluloses

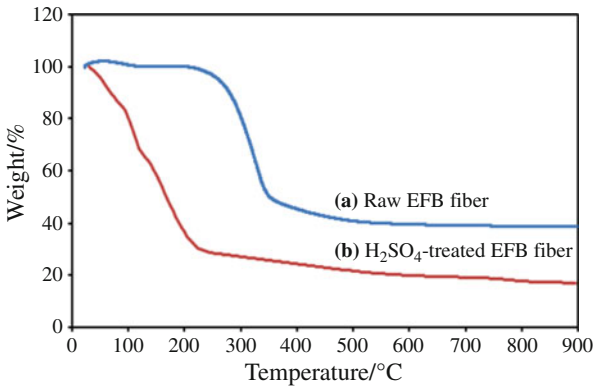

Fig. 1 TG curves for (*a*) raw and (*b*) H_2SO_4-treated EFB fibre during pyrolysis in N_2 gas

accompanied by small mass loss by lignin decomposition. It was then followed by a slow decrement in mass solely due to lignin decomposition [16]. Pyrolysis of hemicelluloses and celluloses occurred rapidly in the range of 220–315 °C and 315–400 °C, respectively, contributed to a sharp drop in the TG profile. On the other hand, a gradual mass loss was observed throughout the TG curve given by decomposition of lignin (in the range 160–900 °C), which was more difficult to be degraded [17]. Thus, continuous slight devolatilisation stage was observed after 350 °C. There is no obvious mass loss observed beyond temperature of 550 °C. Overall, the TG curve of raw EFB fibre in this study agreed well with a typical TG curve of EFB fibre reported by Idris et al. [18].

Sulphuric acid (H_2SO_4) treatment altered the thermal evolution profiles of EFB fibre. The pyrolysis profiles for H_2SO_4-treated EFB fibre were indicated in Figs. 1b and 2, showing the mass loss of the fibre across different temperatures and their corresponding derivative of the mass loss (DTG), respectively. H_2SO_4-treated EFB fibre exhibited three mass losses at temperature less than 250 °C and an almost flat tailing section at higher temperatures. The amount of first mass loss below 85 °C (14.35%) contributed by water vapour evaporation was higher than that of untreated raw EFB fibre. This is due to a more porous and hydrophilic surface after acid treatment which, removed oil content and created pores on the EFB surface by acid attack. Thermal degradation of the H_2SO_4-treated EFB fibre occurred at lower temperatures than that of raw EFB fibre. According to Valix et al. [19], the intercalation reactions of sulphuric acid with the fibre caused a significant thermal decomposition after 100 °C which led to the second mass loss of 20.3%. Both intercalation and exfoliation reactions occurred at temperatures beyond 160 °C [20]. This coincided with the third mass loss (36.61%) for H_2SO_4-treated EFB fibre with a significant mass loss at 160 °C. No obvious mass loss was observed after 250 up to 900 °C. This result agreed with the observation reported by Yang et al. [17], where decomposition of lignin was difficult and occurred gradually up to 900 °C. In other words, the proposed sulphuric acid treatment had brought down the pyrolysis temperature from 350 to 250 °C.

Similarly, thermal characteristics of raw EFB fibre and H_2SO_4-treated EFB fibre in oxidative atmosphere are indicated in Fig. 3. Combustion of raw EFB fibre can be divided into three stages: moisture evaporation, oxidative degradation and combustion of char [15]. Initial mass loss (6.29%) at temperature around 100 °C was attributed to the evaporation of adsorbed water. The subsequence thermal degradations were due to oxidation of the volatile products and followed by the oxidation of charred residue [21]. The oxidative degradation zone of raw EFB fibre occurred in the temperature range of 200–370 °C. A drastic mass loss of 59.36% in this zone was due to a combination of total decomposition of hemicellulose and cellulose, as well as partial decomposition of lignin [22]. The decomposition of the remaining lignin and char oxidation persisted to 370–490 °C [23]. The lignin decomposition of raw EFB fibre proceeded to 900 °C in N_2 atmosphere as reported by Yang et al. [17]. In our case, the constant mass loss from 370 °C persisted also all the way to 900 °C. This may be due to the lignin and char decomposition with the presence of oxygen. The oxidative reaction contributed to the different mass loss profile beyond 370 °C compared to the thermal profile of fibre pyrolysed in nitrogen atmosphere (Fig. 1).

TG and DTG results in Figs. 3 and 4 show three peaks by major mass losses prior to 250 °C and another significant mass loss beyond 450 °C exhibited by H_2SO_4-treated EFB fibre. The first mass loss of 13.24% before 85 °C was attributed to the evaporation of water vapour from the sample. The intercalation of sulphuric acid caused the second mass loss of 19.41% occurred within 85–130 °C. The third major mass loss (38.64%) was due to both intercalation and exfoliation reactions between sulphuric acid and the fibre [19, 20]. With the treatment by sulphuric acid, the end point of volatilisation combustion (370 °C)

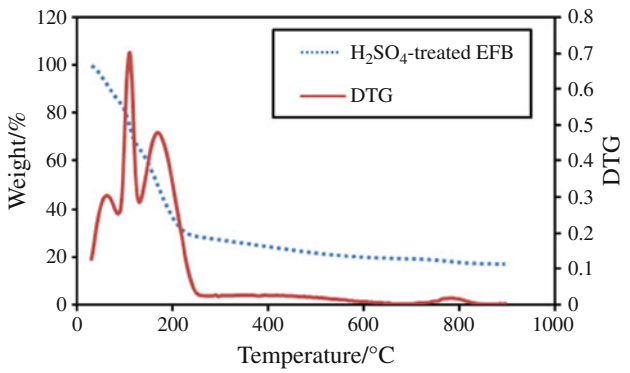

Fig. 2 DTG results for H_2SO_4-treated EFB fibre during pyrolysis

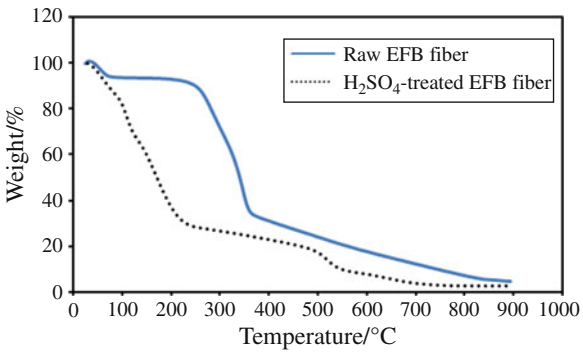

Fig. 3 TG curves for raw and H_2SO_4-treated EFB fibre during combustion

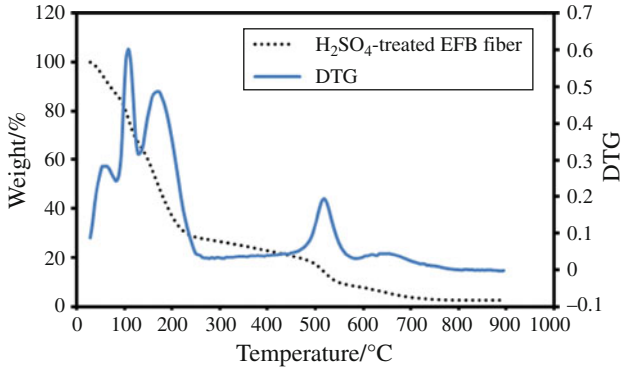

Fig. 4 DTG results for H_2SO_4-treated EFB fibre during combustion

was shifted towards a lower temperature at 250 °C. At 450 °C, the combustion of remaining lignin and carbon residues were facilitated by the treatment with sulphuric acid. As a consequence, the fourth mass loss in chemically treated fibre occurred at a temperature lower than that of raw EFB fibre.

As indicated in Fig. 5, both pyrolysis and combustion behaviours of H_2SO_4-treated EFB fibre were studied in nitrogen and air, respectively. H_2SO_4-treated EFB fibre exhibited similar thermal degradation profiles at lower temperatures ($T \leq 400$ °C) in both nitrogen and air atmospheres. The difference in mass loss was significantly greater at high temperatures ($T \geq 400$ °C) (Fig. 5). From the comparison of the thermal evolution profiles, carbonisation of the H_2SO_4-treated fibre showed higher mass loss after 400 °C. Other than continuous lignin decomposition, oxidative decomposition of carbon residual resulted from combustion of lignocellulosic materials, on H_2SO_4-treated fibre surface with oxygen gas in air caused an extensive mass loss beyond 400 °C. After the cellulosic components in the fibre were volatilised at 400 °C, porosity in char increased. Oxygen diffused easily into char to react with

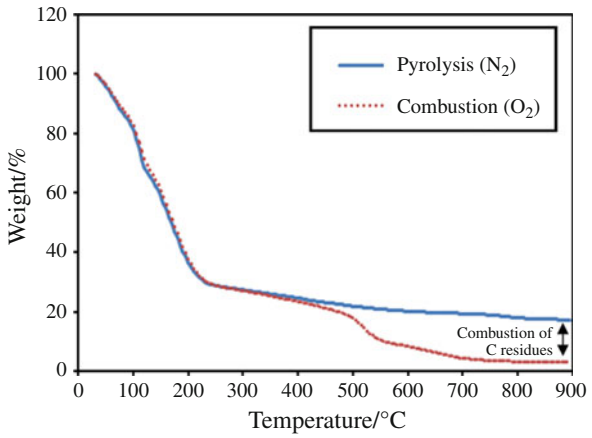

Fig. 5 TG curves for H_2SO_4-treated EFB fibre during pyrolysis and combustion

the carbon residual components in the fibre during combustion [16], resulted a drastic mass loss which was not observed in the N_2 rich pyrolysis. The mass loss difference between pyrolysed and combusted samples was attributed to the amount of carbon residual decomposed in such mechanism.

In short, carbonisation of ACF from EFB fibre could be carried out through combustion in oxidative environment (ambient) at lower temperature, compared to pyrolysis in nitrogen rich atmosphere at higher temperatures. Thus, further carbonisation of the fibre was decided to be carried out in an oxidative environment due to lower carbonisation temperatures. Together with the carbonisation temperatures suggested by Valix et al. [19], our carbonisation temperatures were also identified at 85, 120, 130, 160 and 200 °C from the DTG profile upon completion of each DTG peak.

Surface morphological and microstructural analysis

Figure 6a shows the morphology of raw EFB fibre from cross-section. The cross-sectional image of the raw EFB fibre revealed that it formed by an enormous amount of fibrils. The fibrils could subsequently contribute to high surface area and adsorption sites in the fibre upon activation.

Microstructures of samples EC85H2, EC120H2, EC130H2, EC160H2 and EC200H2 carbonised through combustions in air are shown in Fig. 6b–f. Numerous opening of pore channels were observed at the cross-sectional surface of ACF. Such channels were arranged in an organised two-dimensional structure parallelly similar to the natural channels formed by microfibrils in EFB fibre (Fig. 6a). However, the sizes of pore channels seem to be smaller than that of raw EFB fibre. This may due to the shrinkage of the fibre because of densification caused by dehydration and devolatilisation. Smooth cross-sectional surface of the ACF suggested that the ACF fractured in a brittle mode failure. However, microfibril observed in pore opening of raw EFB fibre could not observed at the cross-section of the ACFs.

Pore characteristics

The pore characteristics of samples EC85H2, EC120H2, EC130H2, EC160H2 and EC200H2 were further discussed by referring to the results obtained from nitrogen adsorption isotherms. The curve of adsorption isotherms provided qualitative information on the adsorption process and a general idea on the pore characteristics of the samples. The isotherms of nitrogen adsorption at 77 K (−196 °C) for samples EC85H2–EC200H2 which were carbonised at 85–200 °C were shown in Fig. 7. All samples exhibited characteristics of type-I isotherm associated with

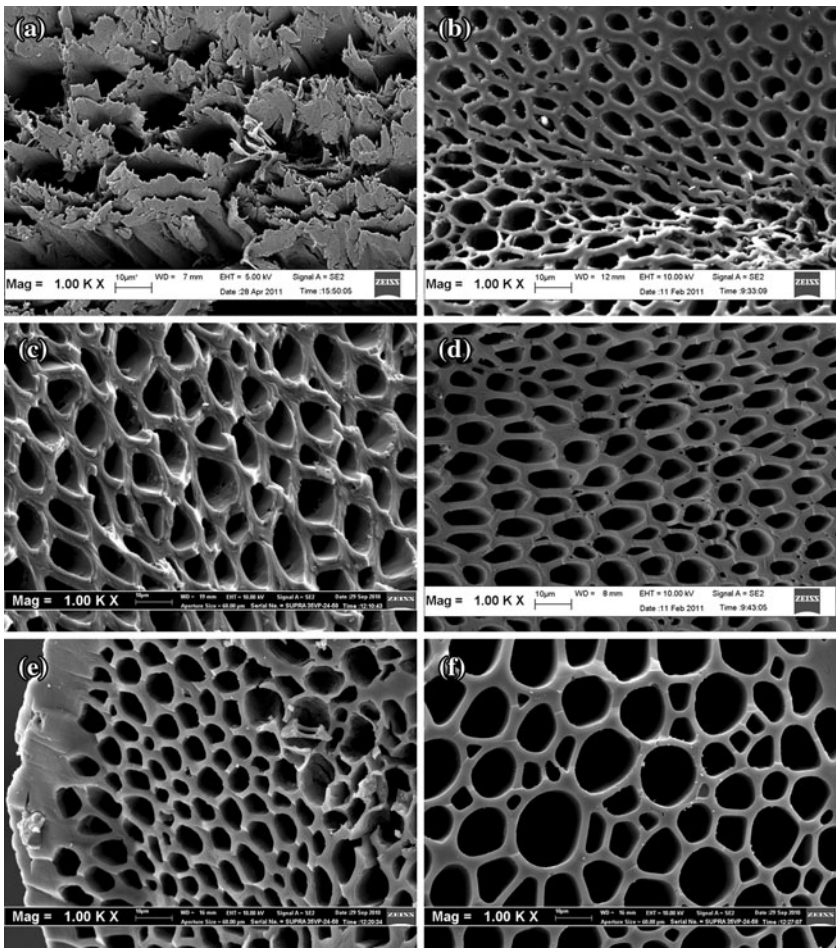

Fig. 6 SEM images of **a** cross-section of raw EFB fibre, **b** EC85H2, **c** EC120H2, **d** EC130H2, **e** EC160H2 and **f** EC200H2

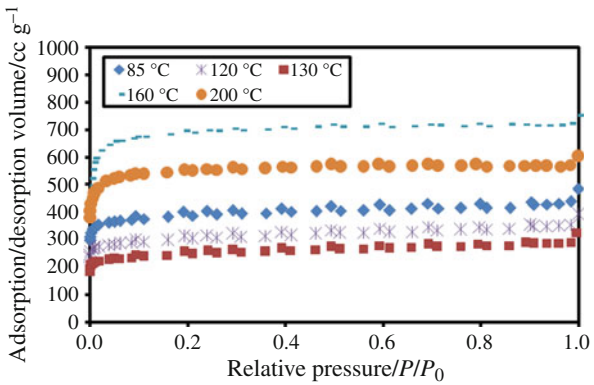

Fig. 7 Adsorption isotherm of nitrogen at −196 °C of samples EC85H2 (85 °C), EC120H2 (120 °C), EC130H2 (130 °C), EC160H2 (160 °C) and EC200H2 (200 °C)

monolayer adsorption of nitrogen gas. The adsorbed amount increased immediately up to a relative pressure of about 0.02 before a plateau was achieved. Very little or nearly no adsorption was observed after that until the isotherms tailed at the end. Large initial nitrogen adsorption capacity took place at low relative pressure (P/P_0) region indicated that the samples were microporous adsorbents. The materials with this typical isotherm normally have an appreciable adsorption amount even at very low relative pressure due to presence of enormous micropores. They had strong interactions in the initial uptake for monolayer coverage, followed by adsorption by micropores. In general, adsorbed amount increased with the increase of combustion temperature. Higher combustion temperatures might result in the removal of more volatile organic matters which generated more micropores.

All samples combusted at temperatures from 85 to 200 °C underwent a carbon dioxide (CO_2) activation at 900 °C for 1 h. CO_2 gas (with kinetics diameter of 3.3 Å) was an efficient activating agent to develop microporosity. This gas caused a steady decrease in the tensile strength to burn-off without changing the fibre diameter significantly [9]. Thus, the shrinkage of ACF observed from SEM micrograph (Fig. 6) was mainly due to carbonisation rather than CO_2 activation. All samples produced by combustion had significant micropores due to such mechanism.

The corresponding pore size distribution (PSD) of samples EC85H2–EC200H2 was estimated by employing HK model [15, 24, 25]. In Fig. 8, the PSD of ACF combusted at lower temperature range (85–200 °C) matched

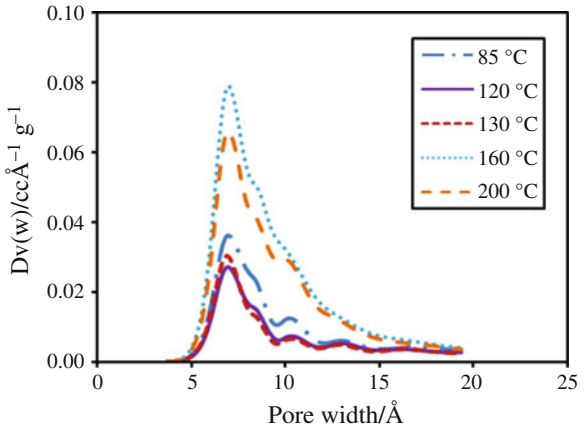

Fig. 8 Pore size distribution of samples EC85H2, EC120H2, EC130H2, EC160H2 and EC200H2

type-I isotherm characteristics which showed the presence of micropores. A uniform pore size of 0.7 nm with narrow PSD (0.5–1 nm) was observed in all the samples produced by combustion. The micropore development was suggested with the intercalation of sulphuric acid into EFB fibre. With heat treatment during carbonisation, the decomposed products of the sulphuric acid may intercalate and force the carbon crystallite layers apart. The internal micropores and surface functional groups containing oxygen were created because these layers remained in their new positions even though the intercalant had been removed [26, 27].

The specific surface area of samples EC85H2–EC200H2 was calculated from the nitrogen adsorption isotherms by applying the BET equation [28]. DR equation was employed to calculate the micropore volume from the N_2 adsorption data [29, 30]. The surface area, micropore volume and total pore volume for all the samples were listed in Table 2.

ACF samples which were carbonised through combustion below 130 °C (EC85H2, EC120H2 and EC130H2) showed decreasing BET surface areas and pore volumes (both micropore volumes and total pore volumes). According to a work which reported the transference of SO_2, O_2 gases and water vapour through a column of activated carbon, by Katagiri et al. [31] in the temperature range from 50 to 140 °C, sulphur dioxide can be oxidised on carbon to form sulphuric acid which was then accumulated in the micropore of carbon. Similarly in our samples, after sulphuric acid treatment, residual sulphuric compounds may remain on the char surface and in the pores. As temperature increased during combustion, more formation of sulphuric acid was promoted from the reaction above, with the presence of water vapour and O_2 from the combustion atmosphere as well as SO_2 from the dissociation of sulphuric source from acid treatment. Higher combustion temperature, produced more sulphuric acid accumulating at the micropores, resulted a lower degree of carbonisation due to limited access of O_2 gas into the micropores filled up by sulphuric acid. Lower degree of carbonisation brought about a lower degree of activation, causing lower surface area and less desirable pore characteristics.

Table 2 Physical properties of samples EC85H2, EC120H2, EC130H2, EC160H2 and EC200H2

Samples	BET surface area/m^{2}g^{-1}	Micropore volume/cc g^{-1}	Total pore volume/cc g^{-1}
EC85H2	1,528	0.634	0.752
EC120H2	1,188	0.505	0.609
EC130H2	955	0.413	0.504
EC160H2	2,743	1.153	1.162
EC200H2	2,184	0.883	0.934

However, a different mechanism applied when the temperature was higher than 150 °C. Surface complexes containing sulphur atoms were formed during sulphuric acid treatment. Compared to sulphuric acid which was formed below 150 °C and filled up the micropores, such sulphuric complexes allowed the access of O_2 gas to the fibre surface which gave rise to a better degree of carbonisation. It has been proven that the removal of sulphur-containing surface complexes took place at 900 °C in the presence of CO_2 [32]. Through this mechanism, higher carbonisation temperature gave a higher degree of carbonisation, provided a better carbonised surface for a more efficient activation and resulted in more preferable pore characteristics. This reaction had possibility to cause the BET surface area and pore volume of sample EC160H2 to be higher than previous samples. Sulphuric acid performed both intercalation and exfoliation reactions beyond 160 °C, which contributed to the excellent pore structure of sample EC200H2 [20].

Conclusions

At lower carbonisation temperature ($T \leq 400$ °C), H_2SO_4-treated EFB fibre exhibited similar thermal degradation profiles in both nitrogen and oxidative atmospheres. The difference in mass loss between pyrolysed and combusted H_2SO_4-treated fibre was attributed to the amount of carbon residual decomposed with the presence of oxygen at higher carbonisation temperature ($T \geq 400$ °C). The amount of nitrogen uptake in ACF decreased with increasing carbonisation temperatures from 85 to 130 °C. This trend may caused by the limited access of O_2 gas into the micropores filled up by excess sulphuric acid resulting a lower degree of carbonisation and activation. ACF that synthesised with higher carbonisation temperature ($T > 150$ °C) performed higher nitrogen uptake than samples EC85H2, EC120H2 and EC130H2.

Acknowledgements The financial supports from USM Short-Term Grant, AUN/SEED-Net RA Grant and SRJP programme, USM Fellowship and USM Research University Postgraduate Research Grant Scheme are highly appreciated.

References

1. Derylo-Marczewska A, Blachnio M, Marczewski AW, Swiatkowski A, Tarasiuk B. Adsorption of selected herbicides from aqueous solutions on activated carbon. J Therm Anal Calorim. 2010;101(2):785–94.
2. Vargas JE, Giraldo L, Moreno-Piraján JC. Enthalpic characterization of activated carbons obtained from *Mucuna mutisiana* with different burn-offs. J Therm Anal Calorim. 2010;102(3):1105–9.
3. Murillo YS, Giraldo L, Moreno-Piraján JC. Determination of partial immersion enthalpy in the interaction of water and activated carbon. J Therm Anal Calorim. 2011;104(2):555–9.
4. Daley MA, Tandon D, Economy J, Hippo EJ. Elucidating the porous structure of activated carbon fibers using direct and indirect methods. Carbon. 1996;34(10):1191–200.
5. Lee SM, Kaneko K. Preparation of ultramicroporous carbon fiber of high adsorption capacity. Carbon. 2003;41(2):374–6.
6. Gao F, Zhao DL, Li Y, Li XG. Preparation and hydrogen storage of activated rayon-based carbon fibers with high specific surface area. J Phys Chem Solids. 2010;71(4):444–7.
7. Im JS, Park SJ, Kim TJ, Kim YH, Lee YS. The study of controlling pore size on electrospun carbon nanofibers for hydrogen adsorption. J Colloid Interface Sci. 2008;318(1):42–9.
8. Carrott PJM, Nabais JMV, Carrott Ribeiro MML, Pajares JA. Preparation of activated carbon fibres from acrylic textile fibres. Carbon. 2001;39:1543–55.
9. Alcañiz-Monge J, Cazorla-Amorós D, Linares-Solano A, Yoshida S, Ova A. Effect of the activating gas on tensile strength and pore structure of pitch-based carbon fibres. Carbon. 1994;32(7):1277–83.
10. Derbyshire F, Andrews R, Jacques D, Jagtoyen M, Kimber G, Rantell T. Synthesis of isotropic carbon fibers and activated carbon fibers from pitch precursors. Fuel. 2001;80(3):345–56.
11. Asakura R, Morita M, Maruyama K, Hatori H, Yamada Y. Preparation of fibrous activated carbons from wood fiber. J Mater Sci. 2004;39(1):201–6.
12. Malaysian Palm Oil Council (MPOC): The Oil Palm Tree. http://www.mpoc.org.my/The_Oil_Palm_Tree.aspx (2011). Accessed 31 May 2011.
13. ASEAN Secretariat: Standards for Oil Palm Fibre. http://www.aseansec.org/7011.htm (2009). Accessed 31 May 2011.
14. Malaysian Industrial Development Authority (MIDA): Felda and TNB to build biomass power plant. http://www.mida.gov.my/en_v2/index.php?mact=News,cntnt01,detail,0&cntnt01articleid=1119&cntnt01returnid=107 (2011). Accessed 21 June 2011.
15. Munir S, Daood SS, Nimmo W, Cunliffe AM, Gibbs BM. Thermal analysis and devolatilization kinetics of cotton stalk, sugar cane bagasse and shea meal under nitrogen and air atmospheres. Bioresour Technol. 2009;100(3):1413–8.
16. Gani A, Naruse I. Effect of cellulose and lignin content on pyrolysis and combustion characteristics for several types of biomass. Renew Energy. 2007;32(4):649–61.
17. Yang H, Yan R, Chen H, Lee DH, Zheng C. Characteristics of hemicellulose, cellulose and lignin pyrolysis. Fuel. 2007;86(12–13):1781–8.
18. Idris SS, Rahman NA, Ismail K, Alias AB, Rashid ZA, Aris MJ. Investigation on thermochemical behaviour of low rank Malaysian coal, oil palm biomass and their blends during pyrolysis via thermogravimetric analysis (TGA). Bioresour Technol. 2010;101(12):4584–92.
19. Valix M, Cheung WH, Zhang K. Role of chemical pre-treatment in the development of super-high surface areas and heteroatom fixation in activated carbons prepared from bagasse. Microporous Mesoporous Mater. 2008;116(1–3):513–23.
20. Petitjean D, Furdin G, Herold A, Dupont Pavlovsky N. New data on graphite intercalation compounds containing $HClO_4$: synthesis and exfoliation. Mol Cryst Liq Cryst Sci Technol A. 1994;244:213–8.
21. Nassar MM, Ashour EA, Wahid SS. Thermal characteristics of bagasse. J Appl Polym Sci. 1996;61(6):885–90.
22. Skreiberg A, Skreiberg O, Sandquist J, Sørum L. TGA and macro-TGA characterisation of biomass fuels and fuel mixtures. Fuel. 2011;90(6):2182–97.
23. Shen DK, Gu S, Luo KH, Bridgwater AV, Fang MX. Kinetic study on thermal decomposition of woods in oxidative environment. Fuel. 2009;88(6):1024–30.
24. Horvath G, Kawazoe K. Method for the calculation of effective pore size distribution in molecular sieve carbon. J Chem Eng Jpn. 1983;16(6):470–5.
25. Duke MC, Pas SJ, Hill AJ, Lin YS, Diniz Da Costa JC. Exposing the molecular sieving architecture of amorphous silica using positron annihilation spectroscopy. Adv Funct Mater. 2008;18(23):3818–26.
26. Lyubchik SB, Benaddi H, Shapranov VV, Beguin F. Activated carbons from chemically treated anthracite. Carbon. 1997;35(1):162–5.
27. Daulan C, Lyubchik SB, Rouzaud JN, Béguin F. Influence of anthracite pretreatment in the preparation of activated carbons. Fuel. 1998;77(6):495–502.
28. Brunauer S, Emmett PH, Teller E. Adsorption of gases in multimolecular layers. J Am Chem Soc. 1938;60(2):309–19.
29. Dubinin NP. Work of Soviet biologists: theoretical genetics. Science. 1947;105(2718):109–12.
30. Legrouri K, Khouya E, Ezzine M, Hannache H, Denoyel R, Pallier R, Naslain R. Production of activated carbon from a new precursor molasses by activation with sulphuric acid. J Hazard Mater. 2005;118(1–3):259–63.
31. Katagiri A, Watanabe K, Yoshizawa S. Reduction of sulfuric acid by hydrogen on activated carbon impregnated with copper sulfate. Bull Chem Soc Jpn. 1981;54(1):1–4.
32. Cuerda-Correa EM, Díaz-Díez MA, Macías-García A, Gañán-Gómez J. Preparation of activated carbons previously treated with sulfuric acid. A study of their adsorption capacity in solution. Appl Surf Sci. 2006;252(17):6042–5.